

Liquid air energy storage (LAES) with packed bed cold thermal storage – From component to system level performance through dynamic modelling

Sciacovelli, Adriano; Vecchi, Andrea; Ding, Yulong

DOI:

[10.1016/j.apenergy.2016.12.118](https://doi.org/10.1016/j.apenergy.2016.12.118)

License:

Creative Commons: Attribution-NonCommercial-NoDerivs (CC BY-NC-ND)

Document Version

Peer reviewed version

Citation for published version (Harvard):

Sciacovelli, A, Vecchi, A & Ding, Y 2017, 'Liquid air energy storage (LAES) with packed bed cold thermal storage – From component to system level performance through dynamic modelling', *Applied Energy*, vol. 190, pp. 84-98. <https://doi.org/10.1016/j.apenergy.2016.12.118>

[Link to publication on Research at Birmingham portal](#)

General rights

Unless a licence is specified above, all rights (including copyright and moral rights) in this document are retained by the authors and/or the copyright holders. The express permission of the copyright holder must be obtained for any use of this material other than for purposes permitted by law.

- Users may freely distribute the URL that is used to identify this publication.
- Users may download and/or print one copy of the publication from the University of Birmingham research portal for the purpose of private study or non-commercial research.
- User may use extracts from the document in line with the concept of 'fair dealing' under the Copyright, Designs and Patents Act 1988 (?)
- Users may not further distribute the material nor use it for the purposes of commercial gain.

Where a licence is displayed above, please note the terms and conditions of the licence govern your use of this document.

When citing, please reference the published version.

Take down policy

While the University of Birmingham exercises care and attention in making items available there are rare occasions when an item has been uploaded in error or has been deemed to be commercially or otherwise sensitive.

If you believe that this is the case for this document, please contact UBIRA@lists.bham.ac.uk providing details and we will remove access to the work immediately and investigate.

Liquid air energy storage (LAES) with packed bed cold thermal storage – From component to system level performance through dynamic modelling

A. Sciacovelli^{a*}, A. Vecchi^a, Y. Ding^a

^aBirmingham Centre for Energy Storage, School of Chemical Engineering, University of Birmingham, Birmingham, B15 2TT, UK

* Corresponding author. Email: a.sciacovelli@bham.ac.uk; Tel. +44 (0)121 415 8866;

Abstract

Energy storage is more important today than ever. It has a key role in storing intermittent electricity from renewable sources – wind, solar and waves – enabling the decarbonisation of the electricity sector. Liquid air energy storage (LAES) is a novel technology for grid scale energy storage in the form of liquid air with the potential to overcome the drawbacks of pumped-hydro and compressed air storage. In this paper we address the performance of next generation LAES standalone plants. Starting our experience with LAES pilot plant at Birmingham (UK), we developed for the first time a validated model to address the dynamic performance of LAES. The model allows us to understand the relationship between component and system level performance through dynamic modelling. We found that the temporary storage of cold thermal energy streams using packed beds improves efficiency of LAES by ~50%. However, due to dynamic cycling charge/discharge, packed beds can bring an undesired 25% increase in the energy expenditure needed to liquefy air. In summary, this work points out that a) dynamics of LAES should not be neglected; b) novel design for cold thermal storage are needed and c) linking component and system level performance is crucial for energy storage.

Nomenclature

D	Inner diameter of packed bed reservoir (m)
D_{out}	Outed diameter of packed bed reservoir (m)
G	Mass flow rate per unit surface ($\text{kg m}^{-2} \text{s}^{-1}$)
H	Height [m]
T	Temperature (K)
U	Overall heat transfer coefficient ($\text{W m}^{-2} \text{K}^{-1}$)
U_V	Overall volumetric heat transfer coefficient ($\text{W m}^{-3} \text{K}^{-1}$)
V	Volume (m^3)
\dot{V}	Volume flow rate ($\text{m}^3 \text{s}^{-1}$)
\dot{W}	Power (W)
Y	Liquid yield (-)
c_p	Specific heat capacity ($\text{J kg}^{-1} \text{K}^{-1}$)
d	Pebble average diameter (m)
h	Specific enthalpy (J kg^{-1})
h_{fs}	Convective heat transfer coefficient ($\text{W m}^{-2} \text{K}^{-1}$)
$h_{fs,V}$	Convective heat transfer coefficient ($\text{W m}^{-2} \text{K}^{-1}$)
j_H	Colburn factor (-)
\dot{m}	Mass flow rate (kg s^{-1})
n	Number of stages (-)
p	Pressure (Pa)
q	Specific heat transfer (J kg^{-1})
q_{CR}	Specific cold recycle (J kg^{-1})
s	Specific entropy ($\text{J kg}^{-1} \text{K}^{-1}$)
t_c	Plant charge time (s)
t_d	Plant discharge time (s)
u_x	Actual velocity (m s^{-1})
v_x	Void shell crossing velocity (m s^{-1})
w	Specific work (J kg^{-1})

x	Coordinate [m]
Re	Reynolds number (-)
Pr	Prandtl number (-)
Greek letters	
α	Heat transfer surface per unit volume (m^{-1})
δ	Thickness [m]
ε	Heat exchanger effectiveness (-)
η_p	Cryogenic pump efficiency (-)
η_s	Isoentropic component efficiency (-)
η_{RT}	Round trip efficiency (-)
η_o	Overall system efficiency (-)
ρ	Density (kg m^{-3})
σ	Void fraction (-)
$\dot{\sigma}_{gen}$	Entropy generation rate [$\text{J kg}^{-1} \text{K}^{-1}$]
τ_c	Dimensionless charging time [-]
τ_d	Dimensionless discharging time [-]
Δ	Thickness (m)
λ	Thermal conductivity ($\text{W m}^{-1} \text{K}^{-1}$)
Φ	Heat flux (W)
Φ_{CR}	Cold recycle (W)
Π	Compression or expansion ratio (-)
ζ	Relative pressure drop (-)
μ	Viscosity (Pa s)

20

21 1 Introduction

22 World-wide renewable energy sources contribute for just 6% [1] of the electricity production while fossil fuel still
23 dominate with a share near 70%. Our society urgently needs to shift toward a more sustainable energy scenario:
24 CO₂ emissions must decrease by 90% by 2050 to limit global warming below 2°C which already severely impacts
25 on our society. To achieve this ambitious target electricity sector needs a full decarbonisation. An intense
26 penetration of renewable energy sources – currently accounting for just 6% of electricity production – will be
27 necessary to meet CO₂ reduction targets. In fact, according to IEA scenarios [1], renewable resources could reach
28 a global share of 65% by 2050. However, such a dramatic increased penetration of intrinsically fluctuating
29 renewables sources – wind and solar in particular – poses major threats to the overall energy system such as
30 imbalance between supply and demand, reduced capacity margin, congestion of networks and in ultimate analysis
31 the need of a more flexible energy system [2]. Among the possible solutions, Energy storage (ES) has great
32 potentials to implement the required flexibility and support a stable energy system [3]. By providing multiple
33 services [3,4] ES enables to capture “wrong time” energy and make it available when required, mitigating the
34 variability of renewables and improving the reliability of the electricity generation asset.

35 Main storage technologies divide in distributed storage – small in nature and suitable for individual users’
36 applications – and bulk storage located in the transmission to provide large scale storage capacity and services
37 according to grid needs. Although distributed storage has seen major developments in recent years [4, 5], bulk
38 energy storage – with 100s of MW power output and storage capacity of hundreds of 100MWh – still relies on
39 pumped hydroelectricity storage (PHS) and compressed air energy storage (CAES) [4, 6]. Both technologies
40 presents severe drawbacks and have limited future development: PHS is geographically constrained, heavily
41 impacts on the environment and shows high capital costs. CAES is limited by the availability of natural
42 underground reservoirs, relatively inefficient compared to electrochemical batteries and it might needs tailored
43 turbomachinery for adiabatic configurations. In recent years an alternative solution for grid-scale storage – namely

liquid air energy storage (LAES) – has drawn the attention of both academic and industry [7-10]. Liquid air energy storage comprises three distinct processes summarized in the schematic of Fig 1: during charging excess electricity – e.g. from wind energy – drives an air liquefaction process based on a Claude cycle. Air from the environment is compressed in stages and then expanded to ambient pressure and sub-ambient temperature to generate the necessary refrigeration effect to liquefy air. Liquid air is then stored in cryogenic tanks at nearly ambient pressure. During discharge pressurized liquid air is regassified and expanded through turbomachines to generate electricity and recover stored energy. Both heat of compression and cold thermal energy from regasification can be stored and recycled to improve the efficiency of the overall system. Thanks to its unique features LAES overcomes the drawbacks of PHS and CAES: it is not geographically constrained, uses commercially available components – thus reduced upfront costs – and it integrates well with traditional power plants [9, 11]. However, LAES needs further research to increase overall efficiency, store cold and hot thermal energy efficiently and increase response time.

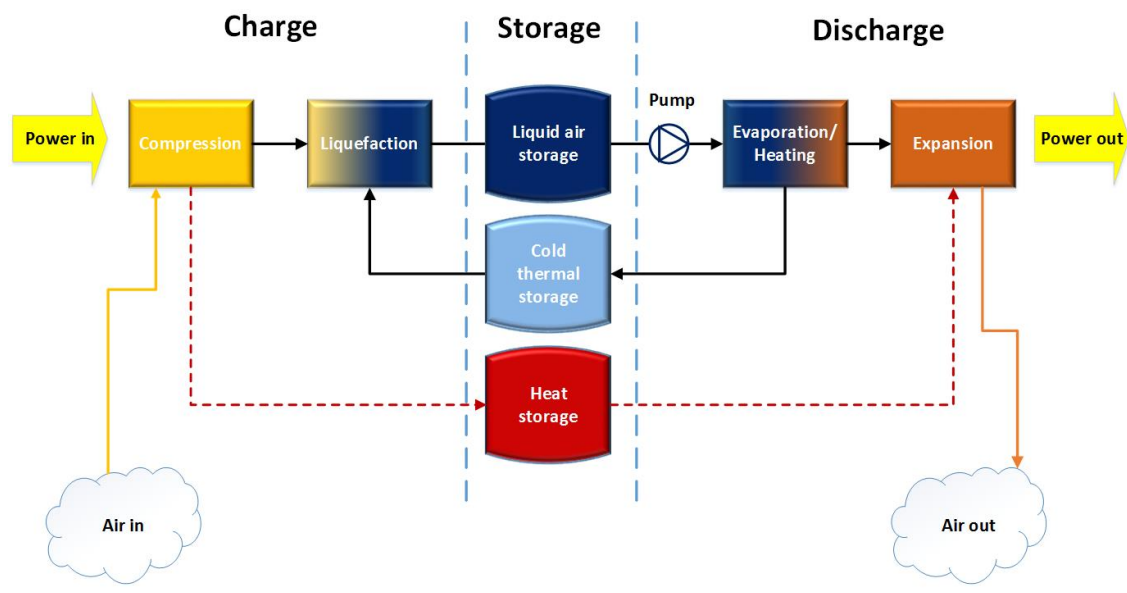


Figure 1: Liquid air energy storage – the concept.

The use of liquid air was firstly proposed at University of Newcastle [12] and tested by Mitsubishi Industries Ltd around 1998 [13] as an extended alternative CAES. In both these studies storage of compressed air was replaced by storage of liquid air but discharge processes still relied on combustor/gas turbine assembly that used regassified air to feed the combustion process. Hence still a pollutant process. In early 2000s researchers at University of Leeds together with Highview Power Storage went on to develop the technology and proposed the key features of LAES [14]. Contrary to Mitsubishi configuration, the system proposed by Highview does not involve any combustion process and uses air as the only working fluid, thus avoiding any pollutant emissions. The design proposed in [14] uses thermal energy storage to recycle cold thermal energy (Fig 1). During discharge cold thermal energy available from liquid air evaporation is stored and subsequently used to reduce refrigeration load to liquefy air during charging process. Such a design change in LAES crucially improves [8] the efficiency of the system, make it pollution free and opens up multiple opportunities for integration of LAES with other energy processes. Progressively, different LAES improvements have been presented [15-17] and a 350kW/2.5MWh pilot plant – now located at the University of Birmingham – was built to demonstrate the feasibility of the proposed design [8]. Cold thermal store was realized using modular packed beds with quartzite rocks [9] and operated at nearly ambient pressure to reduce material costs and diminish plant complexity. The data gathered from the LAES pilot plant

shown that when cold thermal energy is recycled the round trip efficiency of the plant increases of about 50% compared with the case without cold recycle [8].

Although the cold thermal energy storage plays a cornerstone role in LAES, its role and impact on future commercial scale LAES plants remain largely unaddressed. In particular, studies available in the literature do not address a) the *dynamic performance* LAES with cold packed bed thermal storage b) how the cold packed bed thermal storage impact on the operation and performance of the other components of a LAES plant c) the efficiency of stand-alone LAES plant except for the steady-state study presented by Guizzi et al. [10] Such a component-to-plant link is crucial: energy storage systems in future grids with high penetration of renewables will likely operate under variable conditions providing a spectrum of multiple services such as balancing, arbitrage and peak shaving. Thus, steady state analysis under design conditions significantly risk to not capture the realistic operation of energy storage systems. In this work we fill the above mentioned gap in the literature. We present a study of a 100MW/300MWh stand-alone LAES plant with cold packed beds for cold recycle and sensible TES to store heat of compression. The mathematical model we developed includes both algebraic and differential modules that details the transient behaviour of packed bed thermal stores. This allows to link the performance of the thermal storage system with those of the whole LAES plant. To the authors' knowledge the present study is the first of this kind for a LAES plant.

2 Stand-alone liquid air energy storage plant - System description

Figure 2 presents the liquid air energy storage (LAES) plant studied in this work. It comprises three distinct subsystems: the liquefaction unit, the storage unit and the power recovery unit (PRU). During the liquefaction process air is brought to liquid state through a modified Claude process which encompass compression of air and its subsequent expansion to produce the necessary refrigeration effect to liquefy air. Compression is carried out in two intercooled stages (stream 2 to 5 in Fig 2) where heat is stored in sensible form by a diathermic oil that acts both as heat transfer fluid and storage medium (hot storage tanks in Fig 2). The high pressure air stream is then cooled in a multi stream heat exchanger (cold box, stream 3 to 6) by the counter flowing cold (14 to 15) stream of air from the gas/liquid separator and a cold air stream (3C to 4C) from the High grade cold thermal storage (HGCS). Finally, air expands through the cryogenic expander producing a mixture of gaseous and liquid air which are split in the separator, with liquid air collected and stored in a cryogenic tank at about 80K and near ambient pressure. Along the cold box two streams of air – 10 and 12 in Fig 2 – are spilled and expanded in two warm turbo expanders. Extraction at optimal pressure and temperature improves the efficiency of the cooling process (details in Sect. 4.2) by improving the matching of streams temperature profiles in the cold box and thus reducing the power requirement for the liquefaction process. During discharging of LAES plant high pressure and high temperature air expands through a turbine train to generate electricity (stream 15 to 25). At first cryogenic pumps pressurize liquid air withdrawn from cryogenic tank (17 to 18) then liquid air is regassified and reheated in different steps: at the evaporator the cold thermal energy released by liquid air gasification (stream 17 to 18) is captured by counter flowing heat transfer fluid (stream 1C to 2C) and stored into the HGCS. Previous studies and experimental campaign on the of the LAES pilot plant [8] demonstrated that the high grade cold thermal storage can be effectively realized using packed beds with rocks as filler. In such a case the stream 1C-2C consists of gaseous air at nearly ambient pressure which exchange cold thermal energy in the evaporator and stores it in the medium of the packed bed – typically quartzite rocks. Packed beds thermal stores show good thermal efficiency – above 85% [25] – low costs and high safety standards thus are ideal candidates for LAES. Furthermore, HGCS operates at nearly ambient pressure which contributes to reduce balance-of-plant costs (thinner walls for the walls of the HGCS vessel).

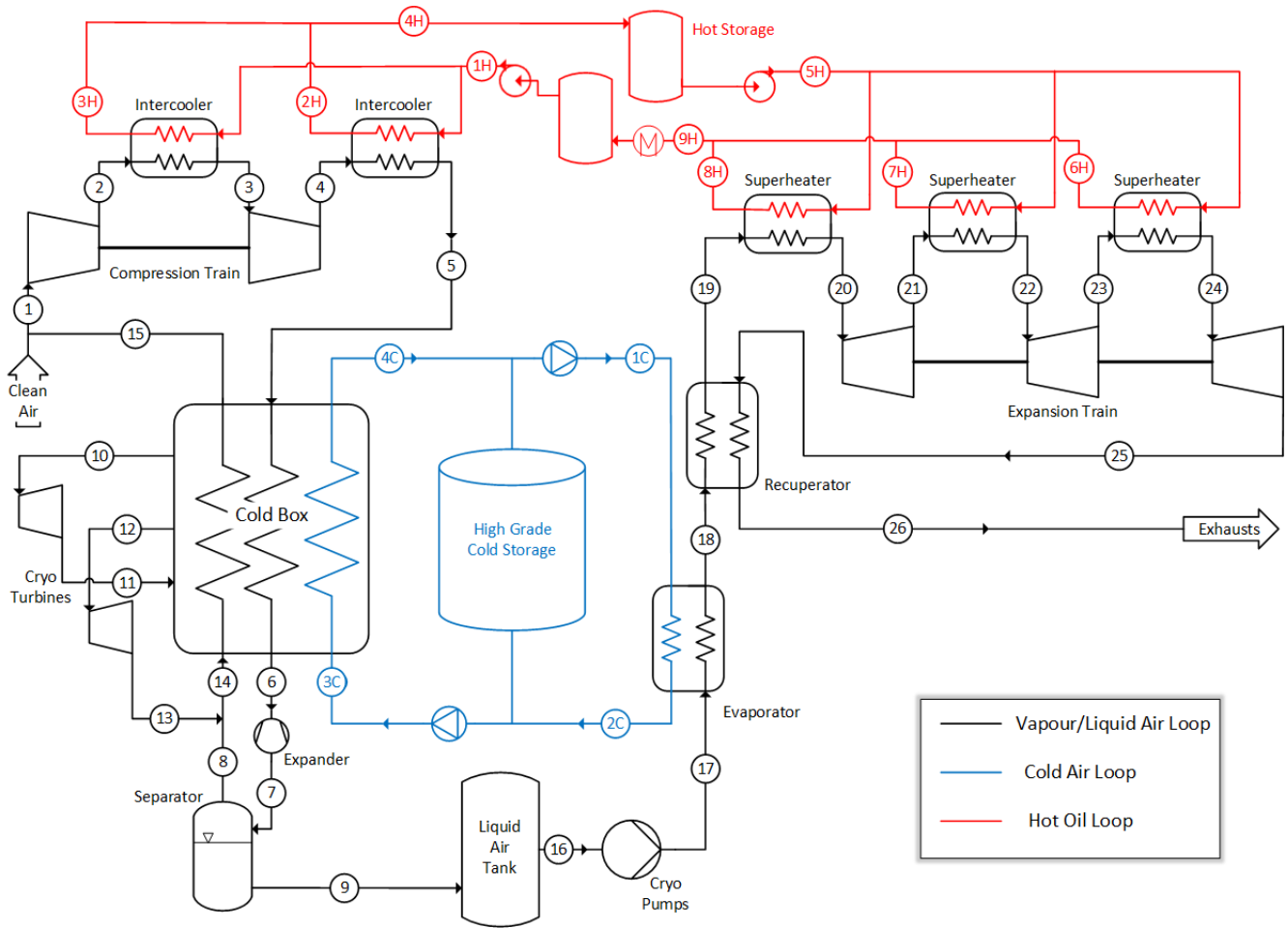


Figure 2: Stand-alone Liquid Air Energy Storage (LAES) plant.

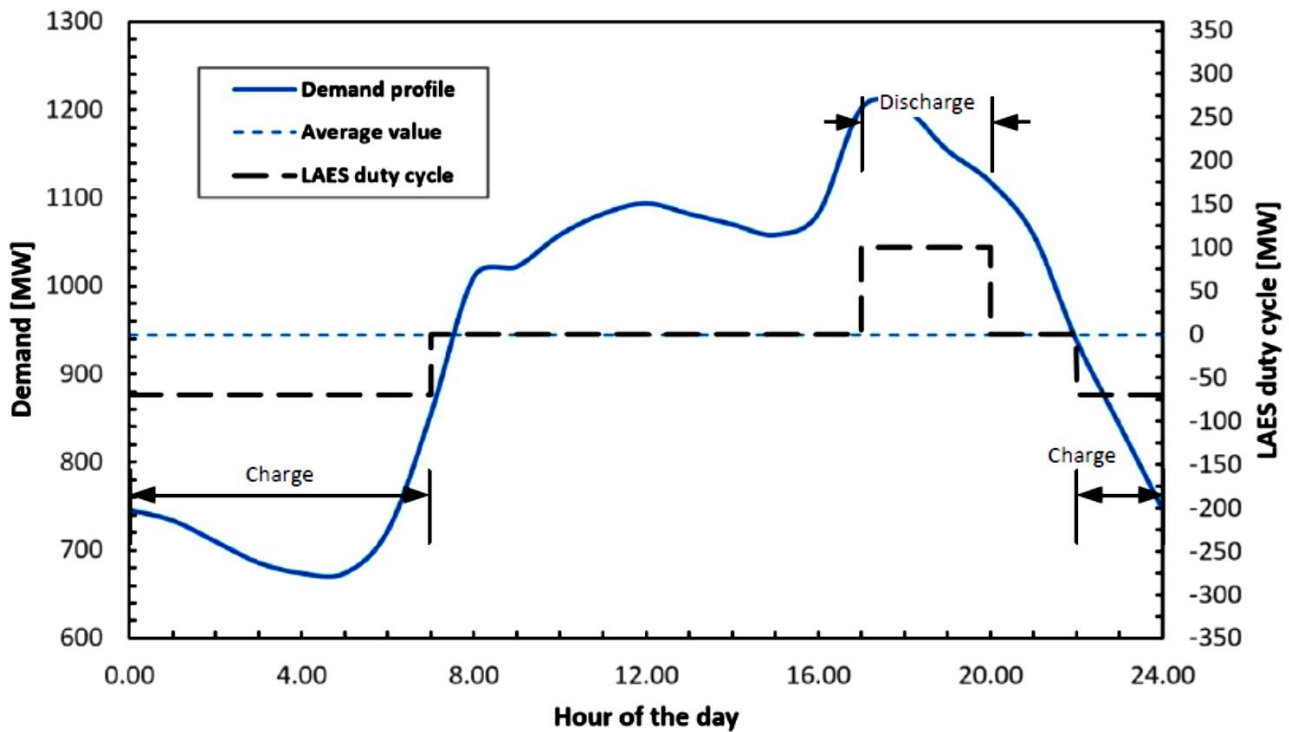
Table 1. Major parameters of standalone LAES system

Quantity	Value
Ambient temperature	288.15 K
Ambient pressure	1.01 bar
Rated power output	100 MW
Energy capacity	300 MWh
Nominal discharge time	3 hours
Compression train rated power	70 MW
Liquid air storage tank	3000 ton
HGCS volume	9200 m ³
Hot thermal oil reservoirs volume	4000 m ³
Compressors isentropic efficiency	85%
Turbines isentropic efficiency	85%
Cryoturbines isentropic efficiency	70%
Cryopumps efficiency	75%
Cold box pinch point temperature difference	5°C

Under nominal conditions the LAES plant provides a power output of 100MW and a storage capacity of 300MWh similarly to other bulk storage technologies [6] – pumped hydroelectricity storage and compressed air energy

122 storage. Figure 3 shows the duty cycle of LAES plant superimposes to the daily electricity demand profile for a
 123 large city for 2030 energy scenario. The daily demand profile was obtained from scenarios reported by National
 124 Grid [18] by scaling down the UK demand profile to large city scale on the basis of city population (1M). LAES
 125 operates in charging mode overnight during a low demand period of 9h while energy is supplied by LAES over a
 126 3h period of peak electricity demand helping in matching demand and supply.

127 Table 1 lists the major design and operational parameters for the charging, storage and discharging units of the
 128 LAES plant under design conditions. The charging and discharging pressure – respectively p_5 and p_{17} in Fig. 2 –
 129 were selected to maximize the efficiency of the LAES plant, as illustrated in detail in Section 4.1. Given the rated
 130 power of the LAES plant axial compressors and turbines were considered; isentropic efficiency of 85% was
 131 selected and a nominal inlet temperature of about 350°C resulted from the storage of the heat of compression
 132 (storage tanks). The oil in the hot thermal store tank is at 375°C (5H in Fig 2) since it recovers the heat of from
 133 the compression train. The complete set of thermodynamic states – enumerated according to Fig 2 – is reported in
 134 Tables 2, 3 and 4. The state points and thermodynamic properties were modelled with EES (Engineering Equation
 135 Solver) coupled with Matlab® using input parameter reported in Table 1; details about the mathematical model
 136 developed in this work are reported in Section 3.



137
 138 Figure 3: Forecasted city daily electricity demand for 2030 superimposed with liquid air energy storage plant
 139 duty cycle.

140
 141 Table 2: Thermodynamic states for the air loop

Point	Mass flow	Pressure	Temperature	Specific enthalpy	Specific Entropy	Quality*
	[kg/s]	[bar]	[K]	[kJ/kg]	[kJ/kgK]	[-]
1	92.33	1.09	286.1	286.3	6.798	-

2	92.33	14.20	642.1	651.9	6.887	-
3	92.33	14.06	298.8	296.1	6.099	-
4	92.33	183.20	673.4	688.9	6.19	-
5	92.33	181.30	299.7	267.7	5.273	-
6	83.10	179.50	96.5	-81.2	3.255	-
7	83.10	1.10	80.0	-97.0	3.339	0.1356
8	11.27	1.10	82.4	79.3	5.523	1
9	71.83	1.10	79.6	-124.7	2.976	0
10	9.23	179.50	220.0	155.9	4.84	-
11	9.23	10.00	110.0	92.5	5.093	-
12	9.23	9.90	130.0	118.6	5.314	-
13	9.23	1.10	82.4	79.3	5.523	1
14	20.50	1.10	82.4	79.3	5.523	1
15	20.50	1.09	278.7	278.9	6.772	-
16	211.80	1.10	79.6	-124.7	2.996	0
17	211.80	75.00	82.9	-113.4	3.031	-
18	211.80	74.25	268.5	249.0	5.46	-
19	211.80	73.51	437.7	434.2	6	-
20	211.80	72.77	613.9	622.0	6.363	-
21	211.80	19.75	454.7	455.6	6.43	-
22	211.80	19.56	619.6	628.0	6.756	-
23	211.80	5.31	459.7	461.8	6.822	-
24	211.80	5.26	621.1	629.7	7.138	-
25	211.80	1.43	461.1	463.5	7.204	-
26	211.80	1.41	277.9	278.0	6.694	-

*when not reported Quality is equal to one.

Table 3: Thermodynamic states for the cold recycle loop

Point	Mass flow	Pressure	Temperature	Specific enthalpy	Specific Entropy	Quality
	[kg/s]	[bar]	[K]	[kJ/kg]	[kJ/kgK]	[-]
1C	406.60	1.50	278.2	278.2	6.677	-
2C	406.60	1.49	92.7	89.4	5.557	-
3C	135.60	1.50	93.0	89.8	5.557	-
4C	135.60	1.49	278.7	278.8	6.682	-

Table 4: Thermodynamic states for the oil loop

Point	Mass flow	Pressure	Temperature
	[kg/s]	[bar]	[K]
1H	90.81	1.10	288.2
2H	47.32	1.09	661.8
3H	43.50	1.09	631.4

4H	90.81	1.09	647.3
5H	274.00	1.10	646.0
6H	91.33	1.09	469.1
7H	91.33	1.09	464.3
8H	91.33	1.09	448.1
9H	274.00	1.09	460.5

146

147 3 Mathematical modelling of LAES plant and validation

148 A hybrid modelling approach was used, enabling to describe in detail the behavior of key components, while
 149 saving computational resources on other parts of the system. Traditional thermodynamic modelling of charge and
 150 discharge processes was carried out using EES software [19]. Mass, momentum and energy conservation equations
 151 for each component have been specified. Routines for thermodynamic properties were already implemented in
 152 EES. A more detailed 1-D, transient model for the packed bed cold storage has been developed using COMSOL
 153 [20]. The cold box was also treated in depth, accounting for both the effect of various fluid streams and pinch
 154 points internal to the heat exchanger. Finally, under MATLAB environment, the different parts of the model were
 155 loaded and run when needed. Model predictive capability was validated against experimental measurements from
 156 the LAES 350 kW pilot plant, located at University of Birmingham. Specific reference to parts of the model is
 157 given in the following sections.

158 3.1 Process components

159 We adopted a steady state model for compressors, turbines, pumps and heat exchangers; for each component we
 160 accounted for mass conservation, energy conservation and entropy balance:

$$161 \quad \sum_i \dot{m}_i = 0 \quad (1)$$

$$162 \quad \Phi - \dot{W}_t = \sum_i \dot{m}_i (h_{out} - h_{in})_i \quad (2)$$

$$163 \quad \sum_j \frac{\Phi_j}{T_j} + \dot{\sigma}_{gen} = \sum_i \dot{m}_i (s_{out} - s_{in})_i \quad (3)$$

164 Isentropic efficiencies $\eta_{i,s}$ have been specified for turbomachinery in order to compute real work and
 165 compression/expansion ratios have been selected as follows:

$$166 \quad \Pi = \sqrt[n]{\left(\frac{p_{MAX}}{p_{min}} \right)} \quad (4)$$

167 where n is the number of stages and p_{MAX} , p_{min} refer to the maximum and minimum pressure of the whole train.
 168 The work input required by cryogenic pumps has been computed as:

$$169 \quad \dot{W}_P = \frac{\dot{V} \Delta p}{\eta_P} \quad (5)$$

170 where \dot{V} is the volumetric flow rate crossing the component and Δp the pressure rise liquid air is subject to.

Two streams heat exchangers were characterized by the effectiveness ε_i , defined as the ratio between the heat actually transferred between streams and its maximum value:

$$\varepsilon_i = \frac{(\dot{m}c_p)_h (T_{in} - T_{out})_h}{(\dot{m}c_p)_{\min} \Delta T_{MAX}} = \frac{(\dot{m}c_p)_c (T_{out} - T_{in})_c}{(\dot{m}c_p)_{\min} \Delta T_{MAX}} \quad (6)$$

Here, the subscript *min* refers to the fluid with minimum heat capacity rate and ΔT_{MAX} is the difference between inlet temperatures of hot and cold stream in the component. Finally, pressure drops in the components were calculated as function of the incoming pressure [10]:

$$p_{i,out} = (1 - \xi_i) p_{i,in} \quad (7)$$

Hot oil loop comprises two storages, where high temperature oil is stored for boosting discharge. While modelling, the hot tank was regarded as adiabatic. Oil mass conservation across both the reservoirs was imposed. As an example, for the hot tank, over a complete charge/discharge cycle it yields:

$$\int_0^{t_c} \dot{m}_{in} dt = \int_0^{t_d} \dot{m}_{out} dt \quad (8)$$

No thermal stratification has been considered in the hot tank, since the inlet oil temperature variation over time was not significant. The temperature at which oil was available at the power recovery unit was thus determined as:

$$T_{oil} = \frac{1}{t_c} \int_0^{t_c} T(t)_{oil,in} dt \quad (9)$$

Hot oil thermodynamic properties used were density $\rho_{oil} = 750 \text{ kg/m}^3$ and specific heat $c_{p,oil} = 2200 \text{ J/kgK}$ [21]

Some performance parameters for the LAES plant were also defined. Roundtrip efficiency was computed as the ratio between the specific work produced w_d and the specific work w_c absorbed by the plant during charging:

$$\eta_{RT} = \frac{w_d}{w_c} \quad (10)$$

Cold recycle Φ_{CR} and specific cold recycle q_{CR} have been defined as:

$$\Phi_{CR} = \dot{m}_l q_{CR} = \dot{m}_{CB} (h_{CB,in} - h_{CB,out}) \quad (11)$$

Where $h_{CB,in}$ and $h_{CB,out}$ refer to the specific enthalpy of air from HGCS, entering and leaving the cold box, and \dot{m}_l is the mass flow rate of liquid generated by the cryogenic cycle. Liquid yield of liquefaction plant is simply given by the ratio between this latter value and the total mass flow rate going through the compression train:

$$Y = \frac{\dot{m}_l}{\dot{m}_{tot}} \quad (12)$$

Dimensionless charge and discharge times were defined, together with a dimensionless axial length for the packed bed:

$$\tau_c = \frac{t}{t_c} \quad \tau_d = \frac{t}{t_d} \quad \Gamma = \frac{x}{H} \quad (13)$$

where t is the time, t_c is the nominal discharge time, t_d is the nominal discharge time and H is the height of the packed bed.

3.2 Cold box

The cold box is a multi-stream heat exchanger which represents the core of the liquefaction system. The presence of several fluid streams, together with the supercritical conditions of incoming air, makes it possible for a pinch point condition to occur at an inner section of the component [22]. To account for this phenomenon, while also taking properly into account the effect of inlet temperature from cold recycle, a specific model was implemented. The approach used is summarized in Figure 4. The heat exchanger was discretized into multiple sections, imposing a fixed temperature drop to the cold stream of about 1°C for each. Given the mass flow rates of both hot and cold streams, together with their temperature at the warm end, the outlet temperature from each section was obtained solving a set of energy balance equations:

$$\begin{aligned} \Phi_h &= \dot{m}_h c_{p,h,i} (T_{h,i} - T_{h,i+1}) \\ \Phi_c &= \dot{m}_c c_{p,c,i} (T_{c,i} - T_{c,i+1}) + \sum_j \dot{m}_j c_{p,j,i} (T_{c,i} - T_{c,i+1}) \end{aligned} \quad (14)$$

$$\Phi_c = \Phi_h$$

On the RHS of Eq. 8 an extra is added to the balance to model the effect of the additional j -th cold stream; we used this approach to account for the cold recycle stream coming from the HGCS and other cold streams. Such modeling approach leads to accurate results for cold box analyses as reported in [23].

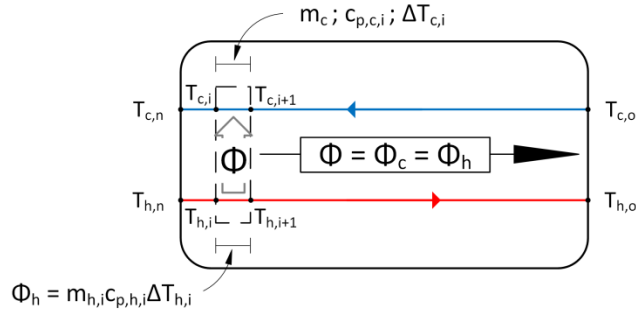


Figure 4. Schematic of modelling approach for the cold box.

3.2 Packed bed cold thermal storage (HGCS)

For the high grade cold thermal storage (HGCS) we adopted a one-dimensional approach to model heat transfer within the packed bed. Energy equations for both solid bed and air were used under the assumption of uniform flow distribution [24,25]:

$$\rho_f c_{p,f} \frac{\partial T_f}{\partial t} + \rho_f c_{p,f} u_x \frac{\partial T_f}{\partial x} = \frac{\partial}{\partial x} \left(\lambda_f \frac{\partial T_f}{\partial x} \right) + h_{fs,V} \frac{1-\sigma}{\sigma} (T_s - T_f) \quad (15)$$

$$\rho_s c_{p,s} \frac{\partial T_s}{\partial t} = \frac{\partial}{\partial x} \left(\lambda_s \frac{\partial T_s}{\partial x} \right) + h_{fs,V} (T_f - T_s) - U_V (T_s - T_\infty) \quad (16)$$

Where subscript f and s stands for fluid and solid. Void fraction σ of the bed was evaluated as function of the ratio particle diameter d_p to packed bed diameter D [25]:

$$\sigma = 0.375 + 0.17 \frac{d_p}{D} + 0.39 \left(\frac{d_p}{D} \right)^2 \quad (17)$$

Equations 15 and 16 are coupled through the volumetric heat transfer coefficient $h_{fs,v}$ which was evaluated using Colburn factor for gas flow in a bed of spheres [26]:

$$j_H = \frac{h_{fs}}{Gc_{p,f}} \text{Pr}^{2/3}$$

$$\sigma j_H = 2.06 \text{Re}_d^{-0.575} \quad (18)$$

$$\text{Re}_d = \frac{\rho_f v_x d}{\mu_f}$$

where h_{fs} is the heat exchange coefficient per unit surface, G_f is the specific flow rate, referred to the void cross sectional area and Pr is the Prantl number. d is the pebble diameter, μ_f fluid viscosity and v_x air velocity. The convective interchange term $h_{fs,v}$ per unit solid volume can be easily computed, recalling the exchange surface per unit volume:

$$\alpha = \frac{6(1-\sigma)}{d} \quad (19)$$

Pressure drop in the systems was computed according to Ergun's correlation [27]:

$$\frac{dp}{dx} = \frac{G^2}{\rho_f d} \left(1.75 \frac{1-\sigma}{\sigma^3} + 150 \frac{1-\sigma}{\sigma^3} \frac{\mu_f}{Gd} \right) \quad (20)$$

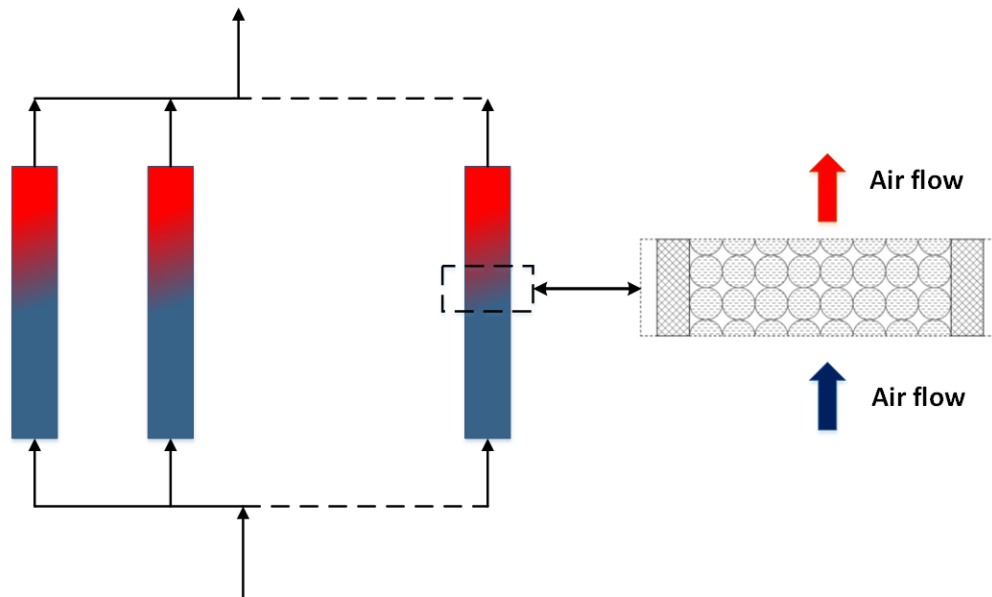
Given the high amount of cold energy to be stored in the standalone LAES, a modular layout was used. The storing volume was segmented in 6 identical cells, each one crossed by one sixth of the total air mas flow rate, according to a parallel layout (Fig 5). Benefits of modularity are linked with system scalability, effective operation at reduced duties and less structural issues [9,28]. In addition, in a LAES system the mass flow rates crossing the the cold storage during plant charge and discharge can differ significantly [28]. A proper pipe arrangement can be used to optimize storage aspect ratio to the mass flow rate, switching from parallel to series connection and vice versa. Just parallel connection between modules was considered in the present case. The transient model (Eqs. 15 and 16) was developed for one single cell; model input parameters are presented in Table 5.

Table 5. Major parameters used for the packed bed model (single cell)

Quantity	Value
D	12 m
d	15 mm
H	13.65 m
σ	0.38
ρ_s	2560 kg/m ³
$c_{p,s}$	541 J/kgK
λ_s	8.99 W/mK
λ_{ins}	0.05 W/mK
δ	15 cm

249

250 The air loop mass flow rate during plant discharge was determined in order to result in a similar temperature
251 difference between cold and hot stream at both ends of the evaporator, once given heat exchanger effectiveness.



252

253 Figure 5. Schematic of modular packed bed high grade cold storage.

254 Thermo-physical of air were evaluated through EES as function of temperature and pressure. For the solid bed, it
255 was observed that thermal properties at cryogenic temperatures differ significantly from the ones at ambient
256 conditions. For this reason, we experimentally measured specific heat and thermal conductivity of quartzite-based
257 river shingle by differential scanning calorimetry (DSC) and laser flash analysis (LFA). Differential scanning
258 calorimetry was performed using Mettler-Toledo DSC2+ with a furnace cooled by means of external chiller which
259 limited the minimum temperature to -80°C . 10mg sample of rocks were tested in aluminum pans from 20°C to $-$
260 80°C at a cooling rate of $5^{\circ}\text{C}/\text{min}$ with samples held at constant $-80^{\circ}\text{C}/20^{\circ}\text{C}$ for 5 min. All the tests were performed
261 under N_2 flow of 20ml/min. The measured specific heat of rocks is presented in Fig 6 left; at cryogenic temperature
262 the specific heat drops by $\sim 20\%$ compared to room temperature highlighting the fact that proper sizing of cold
263 packed bed needs accurate properties measurements at sub-ambient temperature. Although the DSC measurements
264 could not reach temperature of liquid air, they provided useful data that lay in the middle of the expected operating
265 range for the storage.

266 Thermal conductivity was measured using Netzsch LFA 427 laser flash apparatus cooled by liquid nitrogen; each
267 test was conducted with a laser intensity of 480V and laser pulse of 80ms; Cowan method was user to obtain
268 thermal diffusivity from LFA output signal. The thermal conductivity of rocks increases at cryogenic temperatures
269 as shown in Fig 6 right.

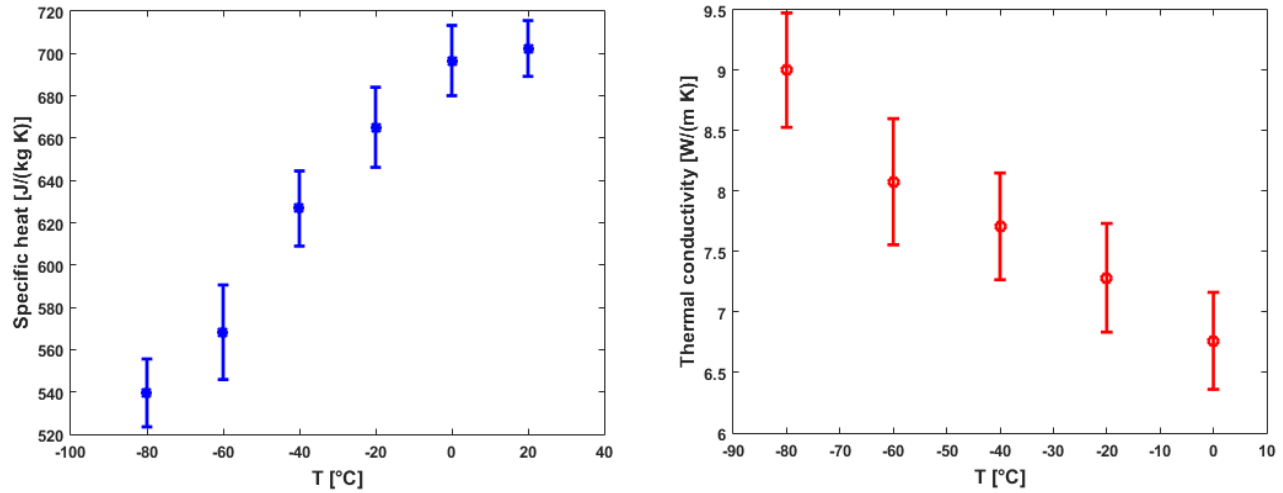


Figure 6. Measured specific heat (left) and thermal conductivity of quartzite-based river shingle (right).

3.3 Model validation

We validated the whole LAES plant model against the experimental data from the first LAES pilot plant originally developed by Highview Powerstorage [11] and currently located at the University of Birmingham, UK (Fig 7). We operated the plant over the period November 2015 – June 2016 and recorded experimental data for the thermodynamic states enumerated in Figs 8 and 9, which details the layout of the plant. Moreover, temperature profile along the high grade cold storage were monitored as well and used to validate the packed bed model presented in Section 3.2. Table 6 shows a nearly perfect match between experimental data and numerical predictions which confirm the reliability of the modeling approach we proposed in Sect. 3. Moreover, the difference between predicted values of enthalpy (presented in Fig. 6) and the values of enthalpy obtained using experimental values for pressure and temperature is within 1.5%, which further confirm the accuracy of the mathematical model. Furthermore, it can be noticed that the pilot plant cryogenic tank operates at 10 bar. Small cryo-tanks (about 50m³ for the pilot plant) are commonly slightly pressurized, however large tanks (e.g. LNG terminals) expected to be used in the LAES plant proposed in Fig. 2 operates near ambient pressure.

The high grade cold storage in the LAES pilot plant is modular packed bed comprising 4 U-shaped cells filled with quartzite rocks as in detail in [28]. Temperature along each cell were recorded during the LAES discharging process and compared with the results from the numerical model of Sect. 3. Figure 10 shows predicted vs. measured temperatures for three different axial locations of the storage. Overall the predictive capability of the model is satisfactorily given the uncertainty on the actual location of thermocouples and some parameters, such as the void fraction.



Figure 7. 350kW/2.5MWh Liquid air energy storage pilot plant at the University of Birmingham, UK.

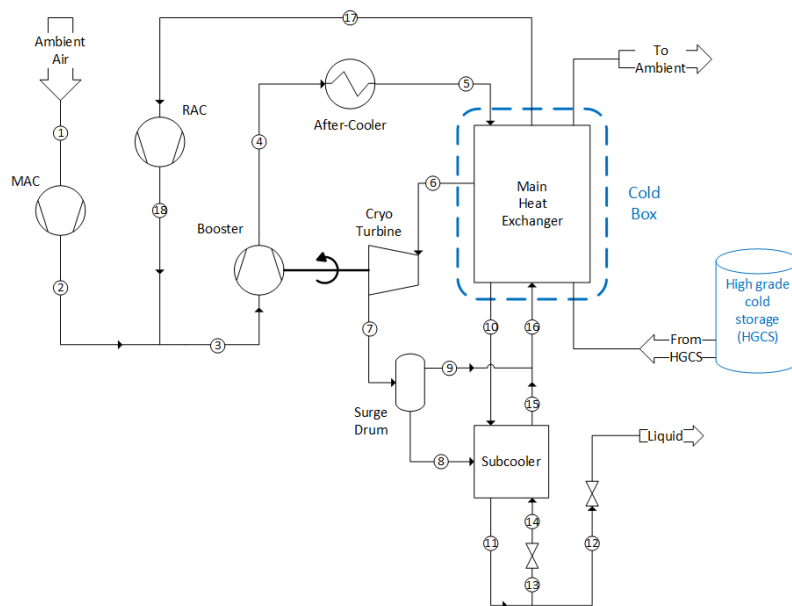


Figure 8. Process flow diagram of the LAES pilot plant – charging process

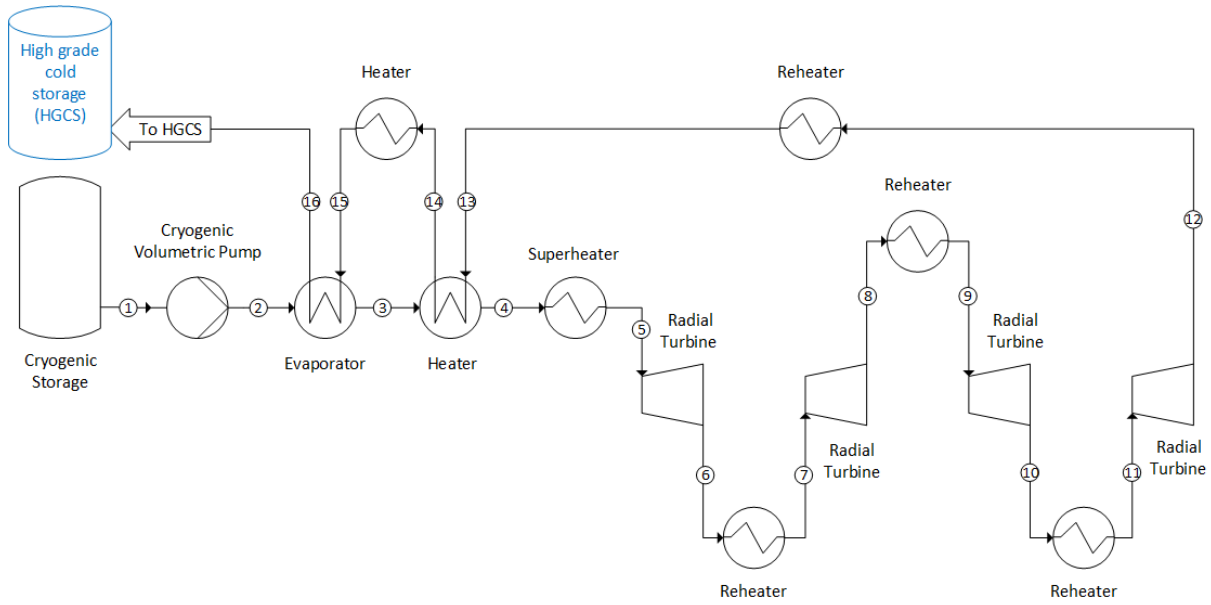


Figure 9. Process flow diagram of the LAES pilot plant – discharging process

Table 6: Thermodynamic states LAES pilot plant; experimental values (grey) vs predicted (white)

Point	p [bar]		T [°C]		\dot{m} [kg/s]	h [kJ/kg]		X [-]
1		10		-169.4		1.84	-64.5	1
2	45.1	46.45	-162.2	-162.5	1.8	1.84	-48.3	-
3		45.1	-91.2	-92.9	1.8	1.84	158.5	-
4		43.7	-16.4	-17.8	1.8	1.84	252	-
5	42.4	43.7	46.3	44.5	1.8	1.84	321.8	-
6		19.5	7.3	9.1	1.8	1.84	288.1	-
7	19	19.5	55	54.9	1.8	1.84	337.2	-
8		10.8	26.6	23.4	1.8	1.84	305.4	-
9	10.6	10.8	45.1	42.8	1.8	1.84	325.9	-
10		4.2	-1.6	-2	1.8	1.84	280.3	-
11	4.1	4.2	44.2	44.5	1.8	1.84	328.9	-
12	1.5	1.5	-2.5	2.7	1.8	1.84	285.9	-
13		1.5	45.2	45.1	1.8	1.84	330.1	-
14		1.5		-44.6	1.8	1.84	236.6	-
15		1.5		37	1.8	1.84	321.6	-
16		1.5	-159.7	-160.3	1.8	1.84	114.8	-

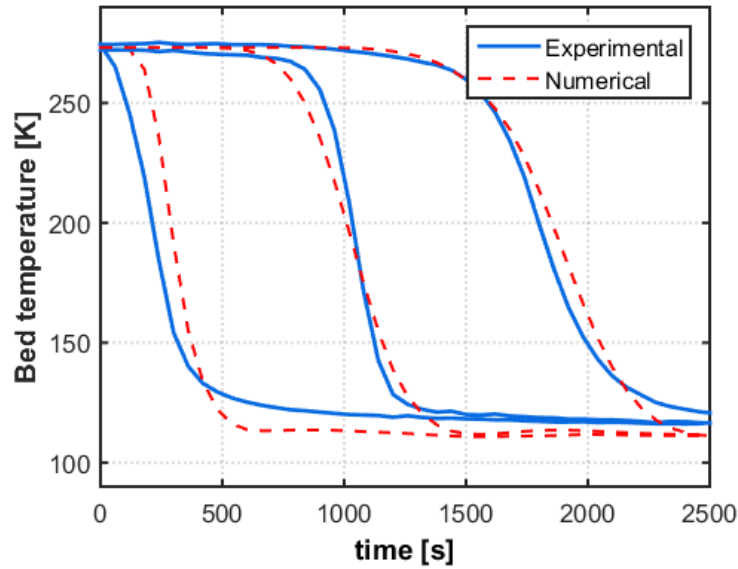


Figure 10. Packed bed model validation; predicted vs measured temperature time evolutions. Data refer to positions at 0.27, 1.7 and 3.13 m along packed bed axis.

4 Results and discussion

This section details the results obtained through the mathematical model presented in Section 3. Firstly, we illustrate and discuss the optimal operation conditions of the plant for steady state operation which lead to the thermodynamic states of Tables 1-3 reported in Section 2. Secondly, we presents the results for dynamic operation of LAES plant and emphasize the link between component performance and plant performance. To this aim, 30 consecutive duty cycles (Fig. 3) were simulated with the full dynamic model.

4.1 Optimal charging and discharging operation conditions

Two major operating parameters affect the performance of LAES plant: a) the charging pressure P_{charge} , namely the compressor outlet pressure during liquefaction process (p_5 in Fig. 2) and b) the discharging pressure P_{disch} , i.e. the turbine inlet pressure during the energy recovery processes (p_{17} in Fig. 2). A variation in either P_{charge} or P_{disch} brings opposite effects; the amount of liquefied air increases as P_{charge} increase but at the expenses of higher compression work. Similarly, the power output from the LAES plant augments if P_{disch} is raised but pumping work from cryogenic pumps increases as well. Clearly, room for optimal selection of pressures exists as Figs. 11 and 12 show. A charging pressure of ~185 bar maximize the round tip efficiency of the LAES plant to about 50% – values consistent with former analysis available in the literature [10]. Above 185 bar the benefits on liquid production are not sufficient to counterbalance the higher expense in compression work as clearly summarized in Fig 12. Above 185 bar liquid yield minimally increases while specific compression work strongly augments. A minimum discrepancy between location of maximum liquid yield and minimum compression work can be observed in Fig 12; we attribute this to the model non-linearity (more than 30 coupled non-linear equations) which makes it sensitive to small variations in the input parameter and in the convergence criteria. However, the region of optimal charging pressure is clearly identified and the validation study previously reported make us highly confident about the results obtained.

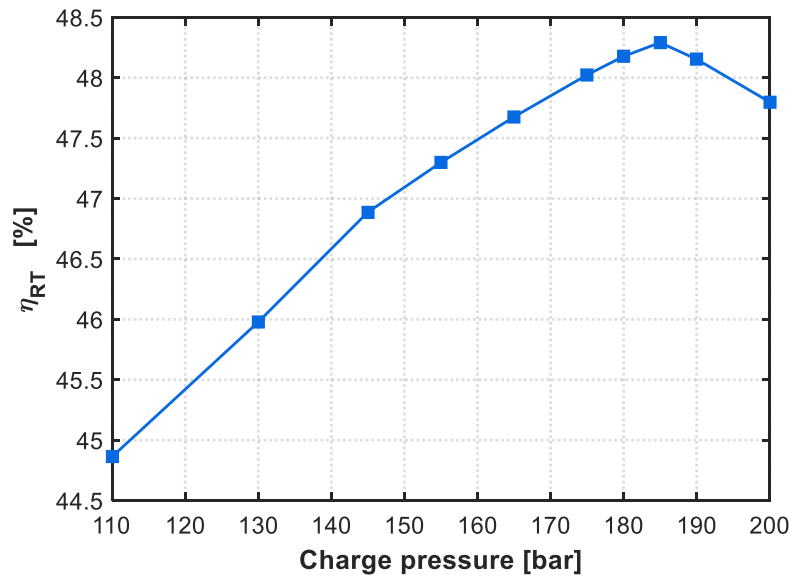


Figure 11. Standalone LAES round trip efficiency for different charging pressures.

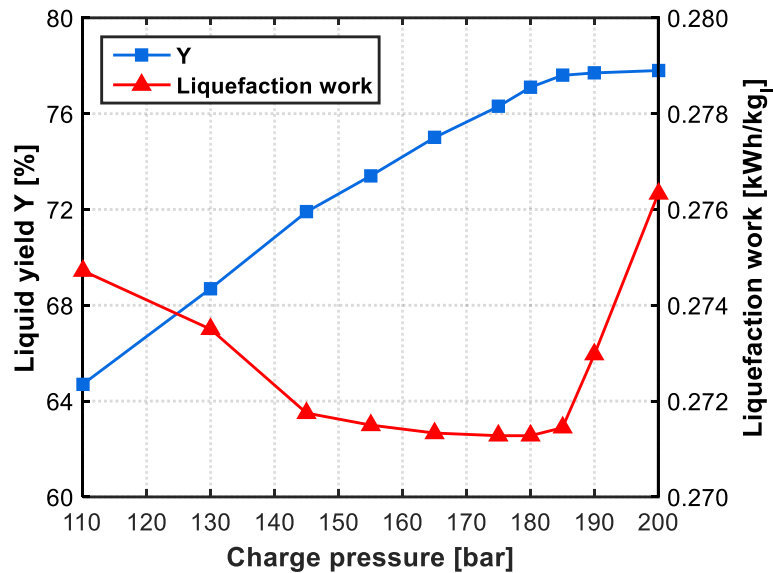


Figure 12. Figures of merits for the liquefaction process as function of charging pressure.

The composite curves for the cold box heat exchanger add further details about the effect of optimal charging pressure. Figure 13 presents three composite curves for three different values of charging pressure across the optimal value of 185 bar. The optimal condition coincides with the best match between temperature profiles of hot stream (5 to 6 Fig 2) and cold streams (14 to 15; 3C to 4C). An optimal charging pressure brings the best possible composite curve in the cold box, thus minimizing the heat transfer irreversibility in the cold box (14, 6 and 3C in Fig. 2). At optimal conditions pinch point locates as close as possible to the cold end of the cold box; different location of pinch point – due to not optimal charging pressure – limits the liquid yield. In particular, pinch point can occur inside the cold box due to variation in specific heat of air at supercritical conditions leading to limitation in heat transfer performance.

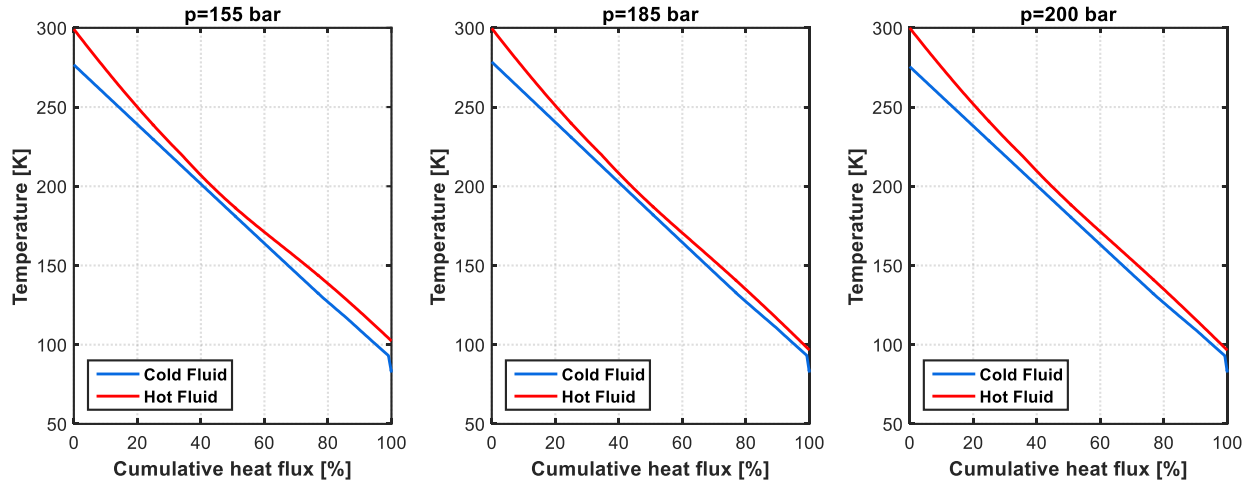


Figure 13: Composite curves in the cold box for different charging pressures.

Beside optimal charging pressure, the amount of air spilled from the cold box and expanded in the cryo-turbines affects the matching of temperature profiles in the cold box as well. Figure 14 illustrates how the spilled mass percentage – i.e. the ratio of cryo-turbine mass flow rate to total air flow rate – can be selected to maximize the liquid yield Y . The optimal spilled mass depends on the value of cold thermal energy recycled through the cold packed bed (stream 3C-4C). Interestingly, a limiting curve exists to which actual curves tend to for high spilled mass percentage. The limiting curve represents the limit that the actual curves will tend to when, for each value of cold recycle, the pinch point exactly occurs at the outlet of the cold box heat exchanger. In fact the limiting curve – continuous line in Fig. 14 – was obtained for pinch point exactly at the cold end of the cold box.

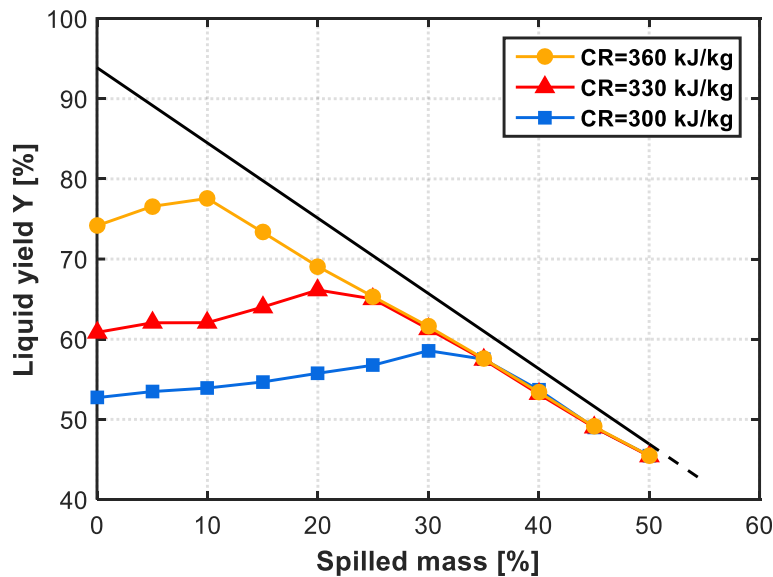
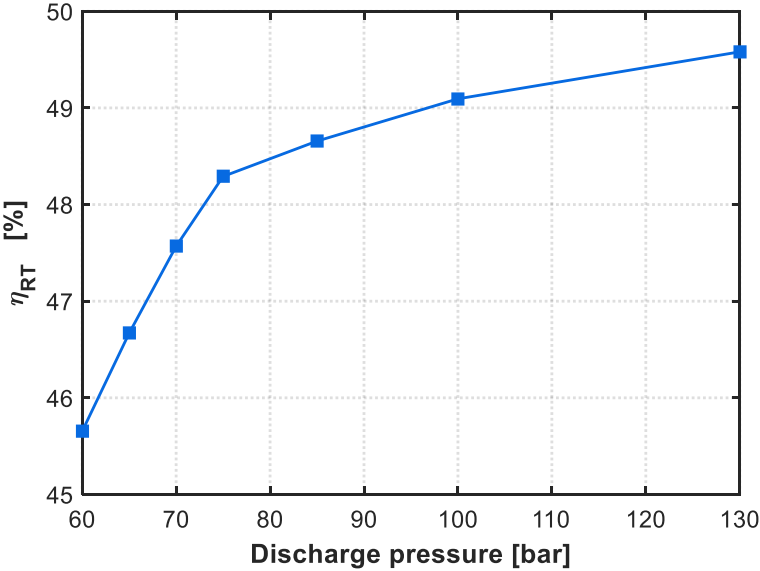


Figure 14: Liquid yield for different spilled fractions; parametrized for different amounts of cold recycled.

As presented in Fig. 15 the round trip efficiency of LAES plant monotonically increases with an increase in the discharge pressure; namely an higher turbine pressure inlet results in a higher specific expansion work. However, increasing P_{disch} lowers the amount of cold could be recycled. This is due to the increase of enthalpy of air at the outlet of the cryopumps caused by the pumping work (Eq. 5). Consequently, the boost in the round trip efficiency becomes marginal after a certain threshold value of P_{disch} : the higher the pressure, the lower the relative benefit

358 achieved, for the same pressure increment, as also pointed out in previous studies [8, 10]. For this reason a
 359 discharge pressure of 75 bar was chosen in this work as design value. Overall, from a comparison of Figs. 11 and
 360 15 the impact of charging and discharging *pressures* on LAES plant performance is comparable although the
 361 compression *work* (70MW) is significantly higher than the pumping *work* (2MW).



362
 363 Figure 15: Standalone LAES round trip efficiency for different discharging pressures.

364 *4.2 Impact of cold recycle on LAES performance*

365 The amount of cold recycled by means of the high grade cold storage (HGCS) is critical to achieve maximum
 366 performance from the LAES plant. As shown in Fig 16, both round trip efficiency and liquid yield dramatically
 367 benefits from an increase in cold recycle: a 16% increase in cold recycle leads to 20% increase in the round trip
 368 efficiency and a 30% increase in the liquid yield. This stems from the key role played by cold recycle into the
 369 overall LAES plant; the cold thermal energy available from gasification of liquid air during discharge is injected
 370 back into liquefaction process (charging) thanks to the HGCS. The latter – as any thermal storage device – allows
 371 to time shift supply and demand of cold into the LAES plant. Without the HGCS, cold thermal energy from
 372 discharge would be otherwise wasted, since the charging and discharging processes do not match in time as shown
 373 in Fig. 3. The cold recycled – from LAES discharge prospective – represents an extra source of cold available at
 374 the cold box (stream 3C-4C in Fig. 2); thus, as shown in Fig 16, it increases the liquid yield at the same power
 375 requirement for air compression. In summary, Fig 16 shows how carefully cold recycle – and its implementation
 376 through the HGCS – should be addressed during the design and operation of a liquid air energy storage plant.

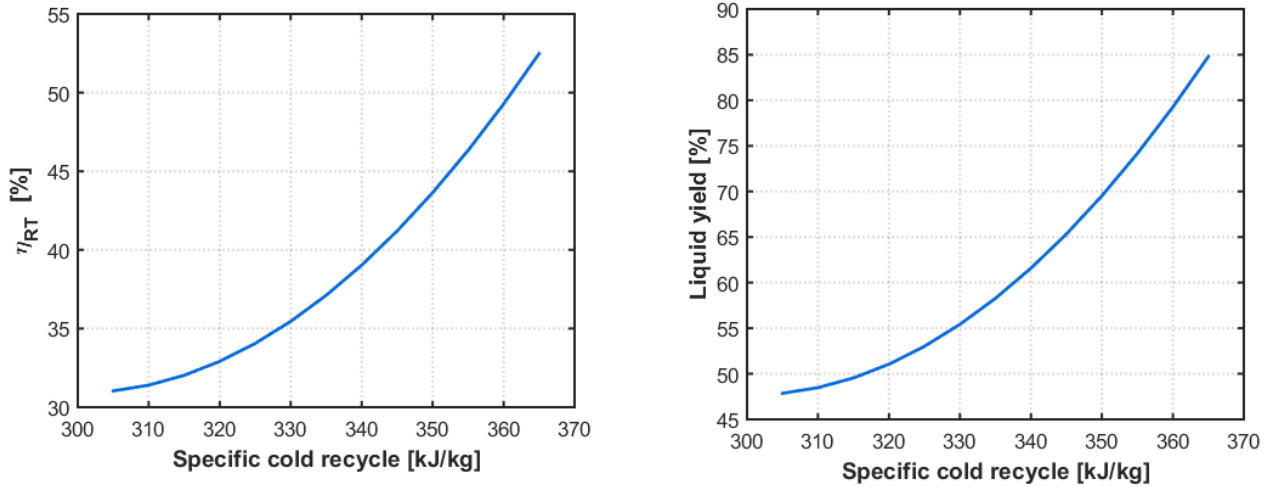


Figure 16: round trip efficiency (left) and liquid yield (right) for different amount of cold recycle.

4.3 LAES dynamic performance – effect of packed bed cold thermal storage on system performance

Over the 30 duty cycles of the LAES plant the high grade cold storage (HGCS) is charged and discharged repetitively. During air liquefaction the HGCS feeds cold thermal energy to the cold box (loop 3C-4C in Fig. 2) improving the performance of the liquefaction process. On the other hand, the HGCS stores the cold thermal energy released by evaporation of liquid air (stream 17 to 18 in Fig. 2) when LAES plant generates electrical power output. Before illustrating the results relative to the HGCS a clarification of the terminology here used is necessary: when LAES plant is *charged* – i.e. air liquefaction occurs – the HGCS *discharges*, namely cold thermal energy is retrieved from the packed bed. On the other hand, as the LAES plant *discharges* – that is the plant generates electricity – the HGCS *charges* by recovering cold thermal energy from evaporation of liquid air. To be consistent with terminology adopted in the previous sections, in the following we will keep using the term *charging* to identify the time span when liquefaction occurs, regardless if referring to the LAES plant or the packed bed cold thermal storage. Similarly, the term *discharging* will be used for both LAES plant and HGCS when referring to the time interval when electric power is generated.

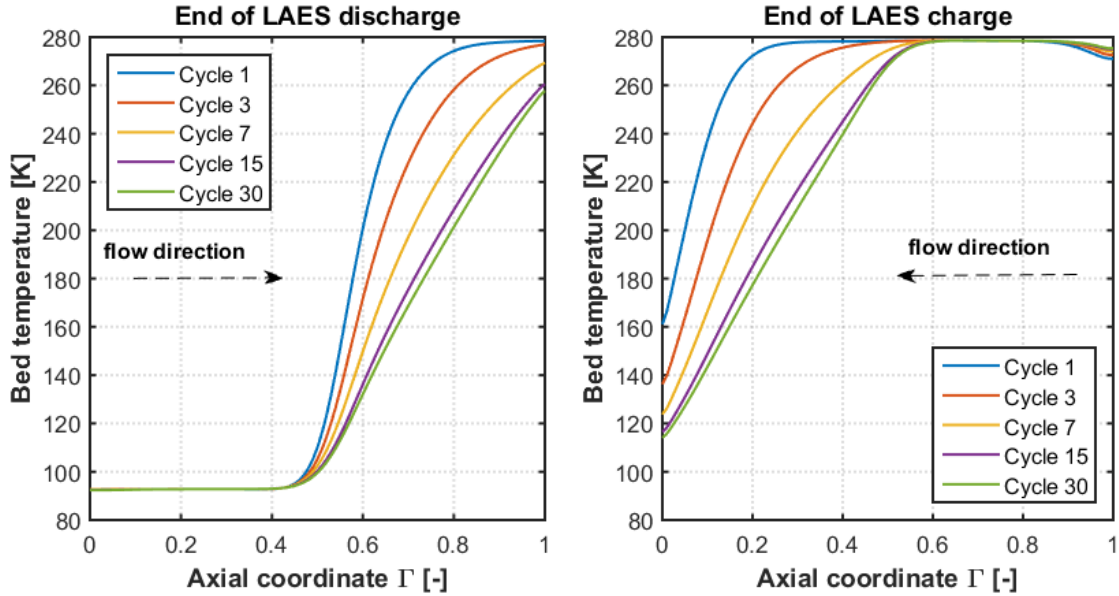


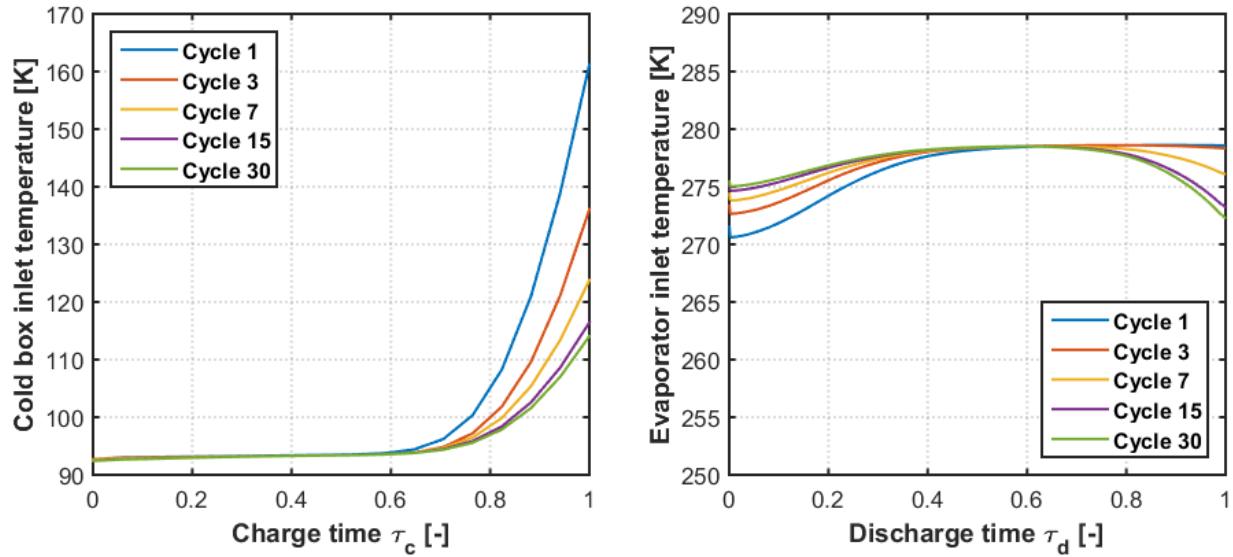
Figure 17: Packed bed temperature profile after LAES discharging (left) and LAES charging (right) for different cycles.

Figure 17 shows the storage temperature profile along the HGCS at the end of discharge and charge, for various cycles. At the end of the first discharge cycle a temperature profile with strong gradient in the range $\Gamma = 0.4-0.6$; this kind of temperature distribution is commonly called thermocline (because of the presence of a strong gradient temperature stratification) which clearly separates the cold extremity of the packed bed from the hot one. However, the temperature stratification rapidly degenerates over the cycles due to axial conduction along the bed and due to periodic charging-discharging of the storage [25]. After 15-20 cycles the evolution of the temperature profile becomes stationary, i.e. the same two profiles establish after charging and discharging. Because of the presence of the thermocline – i.e. a temperature gradient along the packed bed – the outlet temperature from the HGCS during charging ($\Gamma = 0$ in Fig. 17 right) increases over time, as shown in Fig 18. Specifically, the outlet temperature varies when the thermocline approaches the outlet section of the packed bed – due flow air flow rate through the packed bed (in Fig 2 stream 1C-2C during discharge and 3C-4C during charge). Crucially, during discharge the outlet temperature from the HGCS coincides with the cold box inlet temperature (3C in Fig. 2). From Fig 18 it appears that for about 80% of the charging process the system operates under nominal conditions. After that, as the thermocline profile inside the HGCS approaches the outlet, warmer air enters the cold box affecting the liquefaction process and causing a degradation of performance. The effect is far from being negligible; as shown in Fig 19 left, the specific liquefaction work increases by ~25% compared with nominal operating conditions ($\tau_c = 1$) at the end of discharging because of temperature increase at the cold box inlet. The effect is even more relevant before the 15-20th cycle since steady temperature profiles were not established yet in the HGCS.

At the component level, the behaviour of the cold box is directly affected by the inlet temperature from the HGCS. The composite curves – presented in Fig 20 – show that the total heat transfer rates decreases toward the end of charge ($\tau_c = 1$) because the air stream coming from the HGCS warms up. In addition, a higher inlet temperature in the cold box results in a lower outlet temperatures from it, due to the constraint posed by the pinch point; this explains the small drop of the temperature profile at the top of packed bed after discharge ($0.8 < \Gamma < 1$ Fig 17 right).

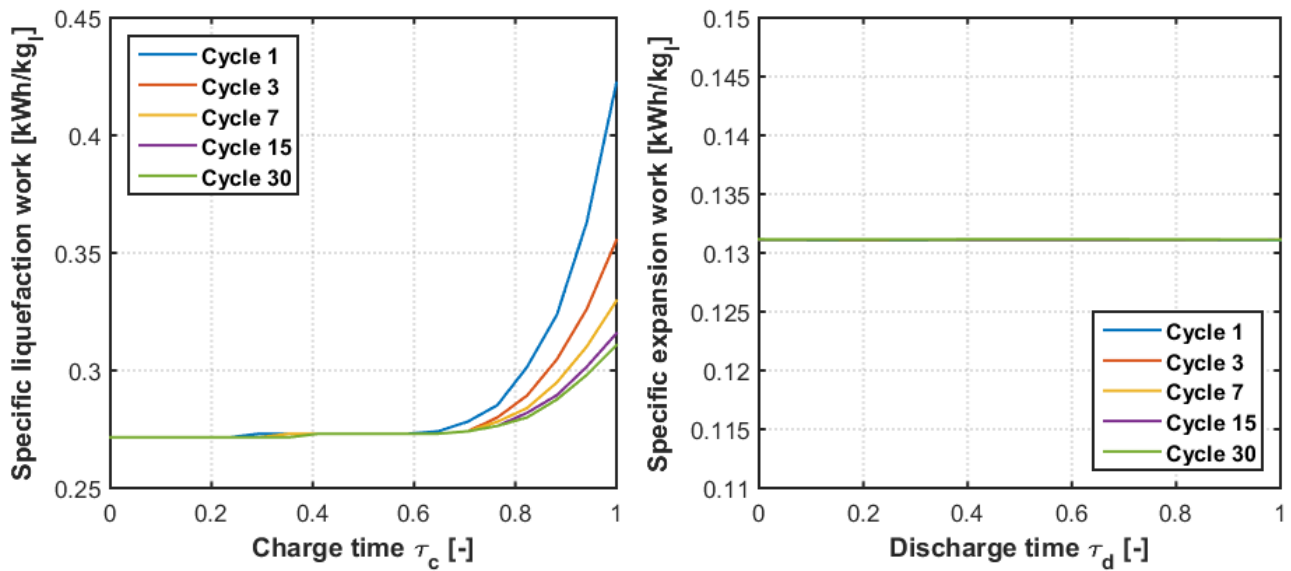
The packed bed cold thermal storage marginally affects the discharging process – i.e. the power recovery from LAES. During discharge the thermocline exits from the top of the HGCS ($\Gamma = 1$ in Fig 17 right); thus the outlet temperature is nearly constant (Fig 18 right) because the temperature profile in the HGCS is nearly flat for $0.4 <$

423 $\Gamma < 1$ in Fig 17 right. Critically, during discharge the packed bed outlet temperature ($\Gamma = 1$ in Fig 17 right) coincides
 424 with the warm inlet temperature of the evaporator (stream 1C in Fig 2) which therefore always operates nearly
 425 design conditions. In fact, the variation of the evaporator warm inlet temperature stays within 10°C as shown in
 426 Fig 18 right. This is beneficial for the LAES discharge since the expansion train constantly operates at nominal
 427 conditions and therefore the specific expansion work does not vary, as illustrated in Fig 19. As a results of the
 428 variation in liquefaction/expansion specific work the round trip efficiency changes from cycle to cycle as
 429 illustrated in Fig 21. After about 20 cycles the efficiency stabilizes around 48% because steady state temperature
 430 profiles establish in the packed bed. Finally, Table 7 summarizes the impact of the cold packed bed thermal stores
 431 impact on the operation and performance of LAES plant.



432

433 Figure 18: time variation of cold box and evaporator inlet temperature; these two inlet temperatures coincide
 434 with packed bed outlet temperature during charge and discharge respectively.



435

436 Figure 19: time variation of specific work for air liquefaction and specific work generated by LAES plant;
 437 variation in work needed liquefaction are caused by time variation of cold box inlet temperature.

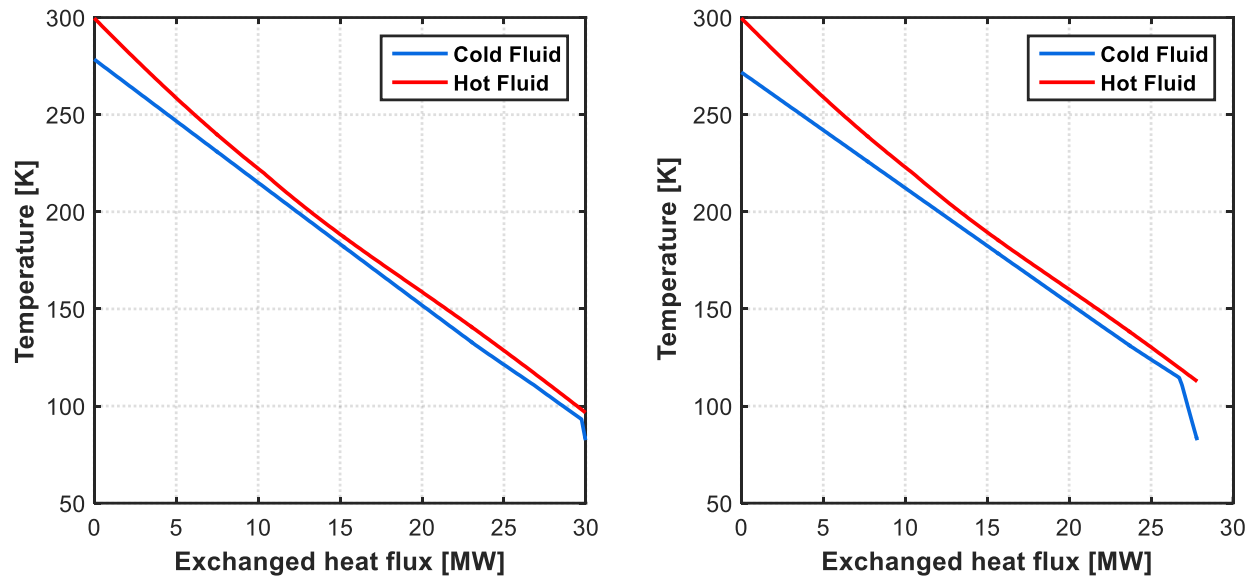


Figure 20. Composite curves in the cold box for $\tau_c = 0$ (left) and $\tau_c = 1$ (right) at cycle 30.

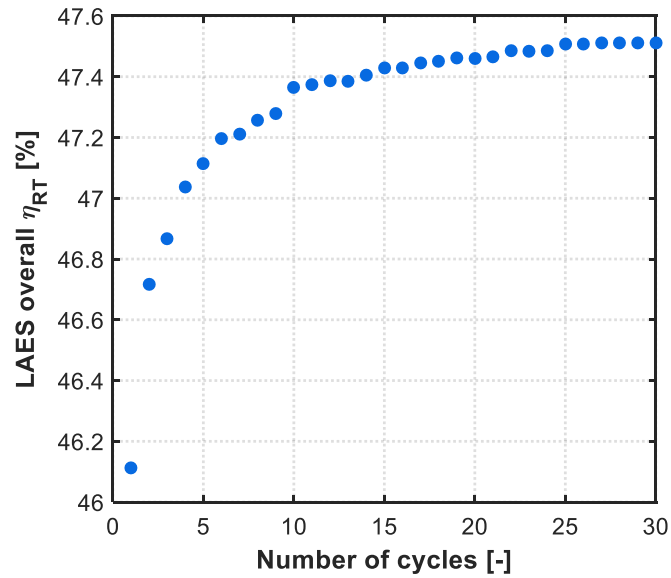


Figure 21. Overall round trip efficiency over the number of cycles.

Table 7: Effect of packed bed cold thermal storage dynamics on LAES plant performance

		$\tau_d \cdot \tau_d = 0$	$\tau_d \cdot \tau_d = 1$	Δ
w_c	[kJ/kg]	977.6	1118.7	14.4
w_d	[kJ/kg]	472.2	472.0	0.0
η	[%]	48.3	42.2	-12.6
Φ	[MW]	25.69	21.70	-15.5
$\Phi_{specific}$	[kJ/kg]	358.8	346.8	-3.4
γ	[%]	77.54	67.02	-13.6

444 5 Conclusions

445 This work presented for the first time a dynamic study of a liquid air energy storage (LAES) plant with rated power
446 of 100MW and storage capacity of 300MWh. We considered a stand-alone plant configuration comprising packed
447 bed thermal energy storage to recycle cold energy from regasification of liquid air and diathermic hot thermal store
448 to capture heat of compression. This was possible by developing an algebraic-differential model detailing the
449 behaviour all the components of LAES plant and in particular the transient feature of packed bed thermal energy
450 storage. The model was validated against experimental results measured from the first LAES plant in the world
451 currently installed at the University of Birmingham. We carried out detailed simulations for consecutive
452 charging/discharging cycles and determined the relationship between component and plant level performance; the
453 following key results were obtained at different levels:

454 *Plant level*

- 455 • The LAES plants achieve a round trip efficiency of 50% under nominal conditions - i.e. a sufficient level
456 of performance for future energy storage technology according to predictions of Strbac et al [29].
- 457 • The recycle of cold from discharging to charging processes reduces the energy required to liquefy air by
458 ~25% – thus efficient cold by recycle by cold thermal storage is the cornerstone subsystem of LAES
- 459 • Optimal charge and discharge pressure should be selected to maximize LAES performance

460 *Cold thermal storage level*

- 461 • Packed bed cold thermal storage with rocks represents a viable solution to implement cold recycle in
462 LAES plants but it introduces dynamic effects due to thermal front propagation in the packed bed.
- 463 • At the end of the discharging process air outlet temperature from the cold thermal store increases by 25%
464 compared with nominal conditions due to degradation of the thermal front in the packed bed;
465 consequently the amount of cold recycled decreased by the same amount.
- 466 • The efficiency of liquefaction process detriments toward the end of each LAES charging cycle due to
467 degradation of the thermal front in the cold packed bed. The degradation of the thermal front manifests
468 as an increase of the air outlet temperature from the cold packed bed reducing the amount of cold recycles

469

470 6 Acknowledgments

471 The authors acknowledge the finance support from Engineering and Physical Sciences Research (EPSRC)
472 Council, UK - SUPERGEN Energy Storage Hub (1EP/L019469/1). The authors would like to thanks Highview
473 Power Storage for the technical support with the LAES pilot plant.

474 References

- 475 [1] 2015 key world energy statistics. IEA - International Energy Agency.
476 <https://www.iea.org/publications/freepublications/publication/key-world-energy-statistics-2015.html>
477 [accessed 05.01.16]
- 478 [2] Carbon Trust - Imperial College London (2015). Can storage help reduce the cost of a future UK electricity
479 system? <https://www.carbontrust.com/resources/reports/technology/energy-storage-report/> [accessed
480 01.08.16]
- 481 [3] EASE/EERA European energy storage technology development roadmap toward 2030 (2013) [http://ease-](http://ease-storage.eu/easeeera-energy-storage-technology-development-roadmap-towards-2030/)
482 [storage.eu/easeeera-energy-storage-technology-development-roadmap-towards-2030/](http://ease-storage.eu/easeeera-energy-storage-technology-development-roadmap-towards-2030/) [accessed 01.08.2016]
- 483 [4] Xing Luo, Jihong Wang, Mark Dooner, Jonathan Clarke. Overview of current development in electrical
484 energy storage technologies and the application potential in power system operation. Applied Energy 2015;
485 137:511–536.

486 [5] T.M.I.Mahlia, T.J.Saktisahdan, A.Jannifar, M.H.Hasan, H.S.C.Matseelar A review of available methods and
487 development on energy storage; technology update. *Renewable and Sustainable Energy Reviews* 33 (2014)
488 532–545

489 [6] Sameer Hameer, Johannes L. van Niekerk. A review of large-scale electrical energy storage. *International*
490 *Journal of Energy Resources* 2015; 39:1179–1195.

491 [7] Bernd Ameal, Christophe T’Joen, Kathleen De Kerpel, Peter De Jaeger, Henk Huisseune, Marnix Van
492 Belleghem, Michel De Paepe. Thermodynamic analysis of energy storage with a liquid air Rankine cycle.
493 *Applied Thermal Engineering* 52 (2013) 130-140

494 [8] Robert Morgan R., Nelmes S., Emma Gibson, Gareth Brett. Liquid air energy storage – Analysis and first
495 results from a pilot scale demonstration plant. *Applied Energy* 137 (2015) 845–853

496 [9] Robert Morgan, Stuard Nelmes, Emma Gibson, Gareth Brett. An analysis of a large-scale liquid air energy
497 storage system. *Proceedings of the Institution of Civil Engineers Energy* 168 May 2015 Issue EN2 Pages 135–
498 144

499 [10] Giuseppe Leo Guizzi, Michele Manno, Ludovica Maria Tolomei, Ruggero Maria Vitali. Thermodynamic
500 analysis of a liquid air energy storage system. *Energy* 93 (2015) 1639-1647

501 [11] <http://www.highview-power.com/> [accessed 01.08.2016]

502 [12] Smith EM. Storage of electrical energy using supercritical liquid air. *ARCHIVE: Proceedings of the*
503 *Institution of Mechanical Engineers* 1847 - 1982 1977; 191: 289-98.

504 [13] Kenji K, Keiichi H, Takahisa A. Development of Generator of Liquid Air Storage Energy System. *Mitsubishi*
505 *Heavy Industries, Ltd Technical Review* 1998; 35: 4.

506 [14] Cheng H, Ding Y, Peters T, Berger F, inventors; Highview Enterprises Limited, assignee. A method of storing
507 energy and a cryogenic energy storage system. WO 2007/096656 A1

508 [15] Morgan R, Nelmes S, Castellucci N, Brett SG, inventors; Highview Enterprises Limited, assignee. Method
509 and apparatus for power storage. WO 2013/034908 A2.

510 [16] Brett SG, Castellucci N, inventors; Method and apparatus in a cryogenic liquefaction process. WO
511 2014/155108 A2

512 [17] Castellucci N, inventor; Highview Enterprises Limited, assignee. Method and system for the re-liquefaction
513 of boil-off gas. WO 2015/063453 A2.

514 [18] National Grid plc; Future Energy Scenarios. www.nationalgrid.com [accessed on 01.08.2016]

515 [19] S. Klein and G. Nellis. Mastering EES; F-chart software, 2014.

516 [20] COMSOL Multiphysics(R); <https://www.comsol.com/comsol-multiphysics>

517 [21] P. Zhao, Y. Dai, and J. Wang. Design and thermodynamic analysis of a hybrid energy storage system based
518 on A-CAES (adiabatic compressed air energy storage) and FESS (flywheel energy storage system) for wind
519 power application. *Energy* 70 (2014), 674–684.

520 [22] G. Venkatarathnam. *Cryogenic mixed refrigerant processes*, Springer, 2008.

521 [23] H. M. Chang, H. S. Lim, and K. H. Choe, Effect of multi-stream heat exchanger on performance of natural
522 gas liquefaction with mixed refrigerant. *Cryogenics (Guildf.)*, vol. 52, no. 12, pp. 642–647, 2012

523 [24] Hitesh Bindra, Pablo Bueno, Jeffrey F. Morris, Reuel Shinnar. Thermal analysis and exergy evaluation of
524 packed bed thermal storage systems. *Applied Thermal Engineering* 2013; 52:255-263.

525 [25] Nicolas Mertens, Falah Alobaid, Lorenz Frigge, Bernd Eppe. Dynamic simulation of integrated rock-bed
526 thermocline storage for concentrated solar power. *Solar Energy* 2014; 110:830–842

527 [26] Bergman, T.L., Lavine, A.S., Incropera, F.P. and D.P. DeWitt, *Introduction to Heat Transfer*, 6th Edition,
528 Wiley, New York, 2011.

529 [27] Ranjit Singh, R.P. Saini, J.S. Saini. Nusselt number and friction factor correlations for packed bed solar energy
530 storage system having large sized elements of different shapes. *Solar Energy* 80 (2006) 760–771

531 [28] Morgan R, Dearman M, inventors; Highview Enterprises Limited, assignee. Method and apparatus for storing
532 thermal energy. US 2013/0240171 A1

533 [29] Strbac G et al. Strategic assessment of the role and value of energy storage systems in the UK low carbon
534 energy future. Report for the Carbon Trust, June 2012, Imperial College, London